Макрогетероциклы
http://mhc-isuct.ru

DOI: 10.6060/mhc245112p

Gas-Phase Structure of 4-(4-Hydroxyphenylazo)phthalonitrile – Precursor for Synthesis of Phthalocyanines with Macrocyclic and Azo Chromophores

Alexander E. Pogonin,[@] Ivan Yu. Kurochkin, Alexander V. Krasnov, Alyona S. Malyasova, Ilya A. Kuzmin, Tatyana V. Tikhomirova, and Georgiy V. Girichev

Ivanovo State University of Chemistry and Technology, 153000 Ivanovo, Russian Federation
[@]Corresponding author E-mail: pogonin@isuct.ru, pogoninalexander@mail.ru

Dedicated to the memory of Academician of the Russian Academy of Sciences Oskar I. Koifman

*The equilibrium structure of free 4-(4-hydroxyphenylazo)phthalonitrile (**p-HPhAPN**, $C_{14}N_4H_8O$) molecules was investigated for the first time by combined gas-phase electron diffraction and mass spectrometry (GED/MS) experiment, as well as through quantum chemical (QC) calculations. It was determined that **p-HPhAPN** in the vapor is represented by planar azo forms. Cis-trans isomerism, azo-hydrazone tautomerism and rotations of different moieties in **p-HPhAPN** were studied in B3LYP-D3/pcseg-2 and DLPNO-CCSD(T0) levels of theory. Electron impact mass spectra of **p-HPhAPN** are typical for azobenzenes and are interpreted using the results of QCxMS calculations at the GFN2-xTB level of theory. Due to the exciting possibility of **p-HPhAPN** in the preparation of phthalocyanines with macrocyclic and azo chromophores, the structures of corresponding isomers of zinc phthalocyanines were investigated.*

Keywords: Phtalonitriles, azophthalonitriles, azo dyes, molecular structure, gas electron diffraction, mass spectrometry, quantum chemistry, phthalocyanines.

Структура молекул 4-(4-гидроксифенилазо)фталонитрила – прекурсора для синтеза фталоцианинов, сочетающих в себе макроциклический и азо- хромофоры

А. Е. Погонин,[@] И. Ю. Курочкин, А. С. Краснов, А. С. Малясова, И. А. Кузьмин, Т. В. Тихомирова, Г. В. Гиричев

Ивановский государственный химико-технологический университет, 153000 Иваново, Российская Федерация
[@]E-mail: pogonin@isuct.ru, pogoninalexander@mail.ru

Посвящается памяти Академика Российской академии наук Оскара Иосифовича Койфмана

*Равновесная структура свободных молекул 4-(4-гидроксифенилазо)фталонитрила (**p-HPhAPN**, $C_{14}N_4H_8O$) была впервые исследована с помощью синхронного электронографического-масс-спектрометрического эксперимента, а также с помощью квантово-химических расчетов. Установлено, что **p-HPhAPN** в паре представлен в виде плоских азо-форм. Цис-транс-изомерия, азо-гидразонная таутомерия и вращения различных фрагментов в **p-HPhAPN** изучены на теоретических уровнях B3LYP-D3/pcseg-2 и DLPNO-CCSD(T0). Масс-спектр электронного удара **p-HPhAPN**, являющийся типичным для производных азобензола, был интерпретирован с использованием QCxMS расчетов на уровне теории GFN2-xTB. В связи с возможностями использования **p-HPhAPN** в получении фталоцианинов, сочетающих в себе макроциклический и азо- хромофоры, исследовано строение соответствующих фталоцианинатов цинка.*

Ключевые слова: Фталонитрилы, азофталонитрилы, азокрасители, молекулярная структура, газовая электронография, масс-спектрометрия, квантовая химия, фталоцианины.

Introduction

Azo dyes R_1-N=N-R_2 are used in different industries – textile, fiber, cosmetic, leather, paint and printing.[1,2] These compounds attract wide attention not only as well-known and popular dyes but also as promising "smart" materials.[3-10] Azo dyes with ionizable groups are also considered as good acid-base indicators[11] displaying different colors in solutions with the change in the p*H* levels. The enormous potential for high-tech industries is explained by their rich photochemistry and the feasibility of modulating their optical properties through conformational switching.[12] The first obvious feature of azo dyes is photochromism caused by *trans* ⇄ *cis* (or *E*- ⇄ *Z*-) isomerization.[13,14] The *E*-isomer is stable. Absorption of photons can cause the formation of the *Z*-isomer. The *Z*-isomers thermally relax back to the *E*-form. Isomerization processes cause significant changes in the geometric structure, dipole and spectral properties.[8,15-17] These aspects can be successfully used to design photo-mechanically responsive materials,[18] optical and photonic devices.[19,20]

Another feature that is specific to hydroxyazo compounds is azo-hydrazone tautomerism[21-24] which determines the possibility of using these compounds to design chemosensing systems.[25,26] The equilibrium between tautomers can be shifted under the influence of environmental factors and the type and position of substituents. Electron-donating substituents in azobenzene derivatives generally stabilize the azo form, electron-withdrawing ones stabilize hydrazone form.[21] Hydrogen-bonding acceptor solvents usually stabilize the azo tautomer, while hydrogen-bonding donor solvents favor the hydrazone tautomer.[27] The authors[22] declare that the azo form should dominate in a gas environment, *i.e.* in the absence of intermolecular bonds. However, there is a clear lack of experimental works on the structure of azo dyes in the gas phase. A suitable experimental method for such studies is the gas electron diffraction (GED) method.[28,29] At the moment, investigations of individual azo dye molecule structures are known only for parent azobenzene (***AB***).[30,31]

Studying the structure of 4-(4-hydroxyphenylazo)phthalonitrile (***p-HPhAPN***, $C_{14}N_4H_8O$, 2NC-Ph-N=N-Ph-OH, 4-[(*E*)-(4'-hydroxyphenyl)diazenyl]phthalonitrile, Figure 1) in the gas phase is the goal of our work. This structural investigation is complicated by possible simultaneous manifestations of *E*- ⇄ *Z*-isomerization, azo-hydrazone tautomerism, and conformational diversity caused by the asymmetrical arrangement of substituent groups. This compound, having the set of features mentioned above, can also be considered as a precursor for the synthesis of phthalocyanines with extended light absorption range.[32,33] Phthalocyanines themselves also represent a huge class of promising compounds that have enormous potential for use.[34-37] Phthalocyanines containing macrocycle and azo chromophores are promising for photodynamic cancer therapy.[32] It is known that conformational properties of initial phtalonitriles can influence the structure of phthalocyanines produced from them.[38,39] Therefore, our study will also be useful for the physical chemistry of phthalocyanines.

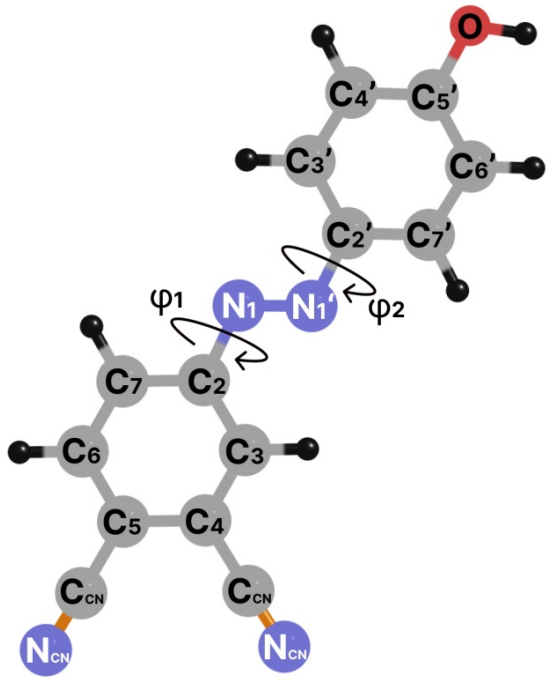

Figure 1. Molecular model of ***p-HPhAPN*** with atom labeling.

Experimental details

Mass-spectrometric experiment

The synthesis of ***p-HPhAPN*** is presented in [32]. The possibility of sublimation of ***p-HPhAPN*** has been previously studied using the MI 1201 commercial magnetic sector mass spectrometer adapted to thermodynamic studies.[40] It was found that in the temperature range of 457–487 K the substance sublime as monomer molecular form without decomposition. Electron ionization results in the appearance of several fragment ions. The electron ionization mass spectra (EI-MS) of the effusing molecular beam is given in Figure 2 and described below (see *Fragmentation of* ***p-HPhAPN***).

Synchronous GED and MS experiment

Evaporation of ***p-HPhAPN*** was performed from a molybdenum effusion cell at a temperature of 464(5) K (measured by W-Re 5/20 thermocouple). Diffraction patterns of vapor ***p-HPhAPN*** as well as MS were recorded on the EMR-100/APDM-1 experimental setup[41,42] at nozzle-to-film distances of 598 and 338 mm. The scattering intensities were recorded on 9×12 cm^2 MACO EM/EMS photographic films. Digitization was performed by a modified microphotometer MD-100 (Carl Zeiss, Jena) setup.[43] Accurate wavelengths of electrons were determined using diffraction patterns for polycrystalline ZnO recorded before and after taking a set of diffraction patterns of a gas. The conditions of synchronous experiments are given in Table S1. EI-MS were recorded simultaneously with the registration of diffraction patterns. The registered EI-MS (Table S2) are in good agreement with the EI-MS previously recorded using MI 1201 equipment (Figure 2).

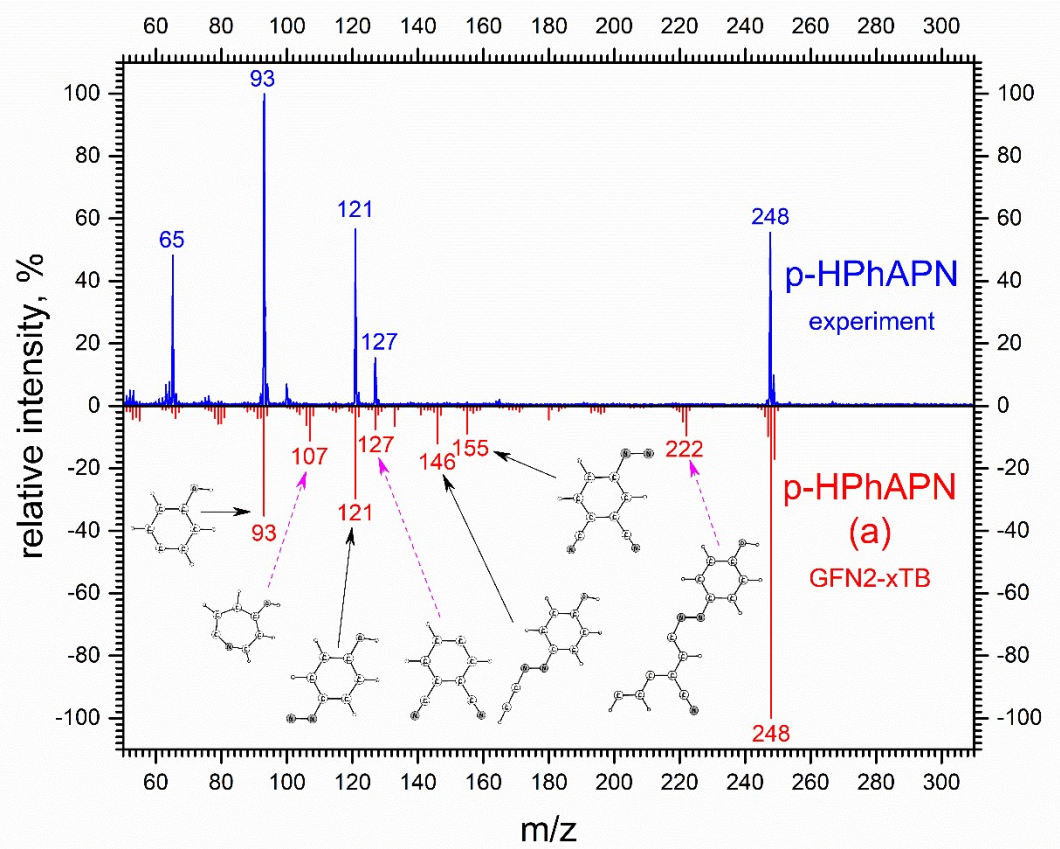

Figure 2. Calculated (GFN2-xTB) EI-MS of ***p-HPhAPN*** in comparison with the experimental EI-MS registered on the equipment MI 1201 at a temperature T=485 K. For assignment black (pink dashed) arrows were used if the contribution of the presented structure to the total intensity is at least (less than) 70%.

Structural analysis

At the beginning of the analysis, we checked the sensitivity of the GED method to different kinds of conformational, tautomeric and isomeric transitions in ***p-HPhAPN***. For this the simulated radial distributions curves *f*(r) were compared (Figure S1). The GED method is sensitive in determining *E* and *Z* isomers. The manifestation of keto-enol tautomerism in ***p-HPhAPN*** is accompanied by a strong rearrangement of both the azo bridge and phenolic/phenolate group. If tautomerism is realized, the GED experiment will record confirmation of this.

The procedure of the GED data refinement was performed using the UNEX program.[44] Z-matrixes for planar structures ***a***, ***c***, ***e***, ***f*** (Figure 3) were constructed according to the C_s-symmetry group (Tables S3-S6). Models based on the structures obtained in QC calculations. The cubic force field was used for the generation of starting vibrational amplitudes and corrections (r_e–r_a) by the VibModule.[45] The regularization approach[46-48] was applied to refine structure parameters in the framework of Equation (1):

$$\chi^2 = \sum_i \left(s_i M(s_i)_{exp} - k_M s_i M(s_i)_{theor}\right)^2 + \\ + \alpha_{reg} \cdot \sum_k w_k \left(p_k^0 - p_k\right)^2 \rightarrow min, \qquad (1)$$

where $s_iM(s_i)_{theor}$ – theoretical molecular scattering intensity; $s_iM(s_i)_{exp}$ – experimental molecular scattering intensity; k_M –the scale factor; α_{reg} – regularization constant; w_k – individual weight function; p_k^0- reference (restraining) value; p_k – is the refined value of *k* structural parameter of the molecule.

The global regularization constant α_{reg} equal to $1 \cdot 10^{-3}$ was chosen in the analysis of dependence $f(\alpha_{reg})$:[49]

$$f = ln^2\left(\frac{\sum_i (s_i M(s_i)_{exp} - k_M s_i M(s_i)_{theor})^2 (\alpha_{reg})}{\alpha_{reg} \cdot \sum_k w_k (p_k^0 - p_k)^2 (\alpha_{reg})}\right), \qquad (2)$$

where $s_iM(s_i)_{theor}$ – theoretical molecular scattering intensity; $s_iM(s_i)_{exp}$ – experimental molecular scattering intensity; k_M – the scale factor; α_{reg} – regularization constant; w_k – individual weight function; p_k^0 – reference (restraining) value; p_k – the refined value of *k* structural parameter of the molecule.

The weights of the parameters in the Equation (1) were obtained ($w_k = \sigma_k^{-2}$) from their ascribed standard deviations (σ_k): 0.005 Å for bond lengths, 0.5° for valence and dihedral angles. In least squares (LS) analysis the weighted disagreement factor (wR_d) between experimental and theoretical scattering intensity was calculated as

$$wR_d = \sqrt{\frac{\sum_{i=1}^{N} w_i (s_i M(s_i)_{exp} - k_M s_i M(s_i)_{theor})^2}{\sum_{i=1}^{N} w_i (s_i M(s_i)_{exp})^2}} \cdot 100\%, \qquad (3)$$

where $s_iM(s_i)_{theor}$ – theoretical molecular scattering intensity; $s_iM(s_i)_{exp}$ – experimental molecular scattering intensity; k_M – the scale factor; w_i – the weight of $sM(s)$ calculated from the respective standard deviation as $1/\sigma^2$; unweighted disagreement factor $R_f = wR_d$ with all w_i=1. The following values were used in our refinement: w_i=1 for s_i=[1.3; 19.9] Å^{-1}; σ=2 for s_i=[20.0; 27.6] Å^{-1}.

Computational details

DFT calculations of molecular geometries and Hessian of ***p-HPhAPN*** were performed using the Gaussian 09 program package.[50] B3LYP[51,52] functional with Grimme's dispersion corrections D3[53] and pcseg-2[54] basis set from the Basis Set

Exchange software[55] were used. This basis set was optimized using a density functional BLYP and was recommended in calculations of geometries, vibrational frequencies[56] and general-purpose ground state thermochemistry.[57] "Tight" optimization convergence criterion and an "ultrafine" grid (pruned, 99 radial shells and 590 angular points per shell) were used. QTAIM (Quantum theory of atoms in molecules) analysis was performed using AIMAll software package.[58]

The domain-based local pair natural orbital coupled cluster method with single, double and semi-canonical perturbative triples corrections DLPNO-CCSD(T0)[59-62] with TightPNO thresholds has been used for single-point (SP) energy calculations in ORCA program[63] for geometries optimized at B3LYP-D3/pcseg-2 theory level. SCF convergence was set to 'VeryTight'. Although DLPNO-CCSD(T0/T1) is indeed possible to use for a wide range of molecules,[64,65] this step in calculations is still computationally expensive. For example of ***p-HPhAPN***, the ratio of computational time of SP calculations at DLPNO-CCSD(T0) with cc-pVTZ[66] and cc-pVQZ[66] basis sets to CPU time of B3LYP/cc-pVTZ SP calculation are *ca*. 14 and 90, respectively. To ensure reliability and feasibility of the calculations carried out, two-point complete basis set (CBS) extrapolation Equality (4)[67] was employed:

$$E^{n}_{DLPNO-CCSD(T0)} = E^{\infty}_{DLPNO-CCSD(T0)} + \frac{A}{(n+1/2)^4}, \quad (4)$$

where n=3 for cc-pVTZ and n=4 for cc-pVQZ, A is the constant to be found through a solution of a system of linear equations.

This scheme was recommended[68] for routine predictions in gas-phase thermochemistry of simple organic compounds. The calculations utilize cc-pVTZ and cc-pVQZ basis sets.[66] The auxiliary basis sets cc-pVnZ/C[69] required for the resolution of identity (RI) approximation were employed.

The electron ionization mass spectra (EI-MS) of azobenzene (***AB***) and ***p-HPhAPN*** were simulated by the QCxMS program[70,71] using Born-Oppenheimer molecular dynamics (MD) at the GFN2-xTB[72] level of theory. The calculations were carried out using the following settings: maximum MD time – 10 ps, initial temperature – 470 K, impact excess energy per atom – 0.6 eV/atom, electron-beam impact energy – 50 eV, number of trajectories – 600 and 675 for ***AB*** and ***p-HPhAPN***, respectively.

Results and Discussion

Conformational and isomeric analysis

The DFT study of the ***p-HPhAPN*** molecular structure was carried out based on the probable manifestations of (i) *cis-trans* isomerism, (ii) tautomerism, (iii) rotations of substituted phenyl rings around N1-C2 and N1'-C2' bonds, (iv) rotation of O-H group around C-O bond. In this regard, 16 structures (***a-h***, ***za-zh***) were found and studied (Figure 3). The planar structure ***a*** of C_s symmetry corresponds to minimal energy on the potential energy surface (PES). It is characterized by the cisoid location of the -CN groups and transoid location of hydrogen atom H5' (see Figure 1) relative to the chain C5···N1-N1'···C5'. However, the relative energies of structures with different arrangements of these cyano- groups and the hydrogen atom are negligible and do not exceed 1 kJ·mol^{-1}. The Z-isomers (***za-zh***, Figure 3) are higher in energy, which is typical for the parent ***AB*** and a large number of other azo dyes. The energy benefit of the E-isomers is explained by the presence of a large delocalized π-system.[17,73] Orbital conjugation of the phenyl rings and azo bridge in the Z isomers is less pronounced. Steric repulsion of neighboring phenyl groups is also exhibited in Z-isomers, which also makes this structure to be less favorable than E-isomers.[17]

In the case of migration of a hydrogen atom from oxygen atom to an azo-bridge (enol→keto), phthalonitrile fragment changes slightly and aromaticity is retained (Table S7). However, the second ring changes its structure radically. C3'-C4' and C6'-C7' bond lengths are decreased from 1.38 Å to 1.34 Å. The remaining C'-C' bonds become single. The electron delocalization index of the N1-N1' bond decreases from 1.86 for model ***a*** to 1.38 and 1.48 for ***e*** and ***g*** structures (Table S8). Thus, in the keto-isomers there is no any delocalized π-electron system throughout the whole molecule, which makes these structures less energetically favorable.

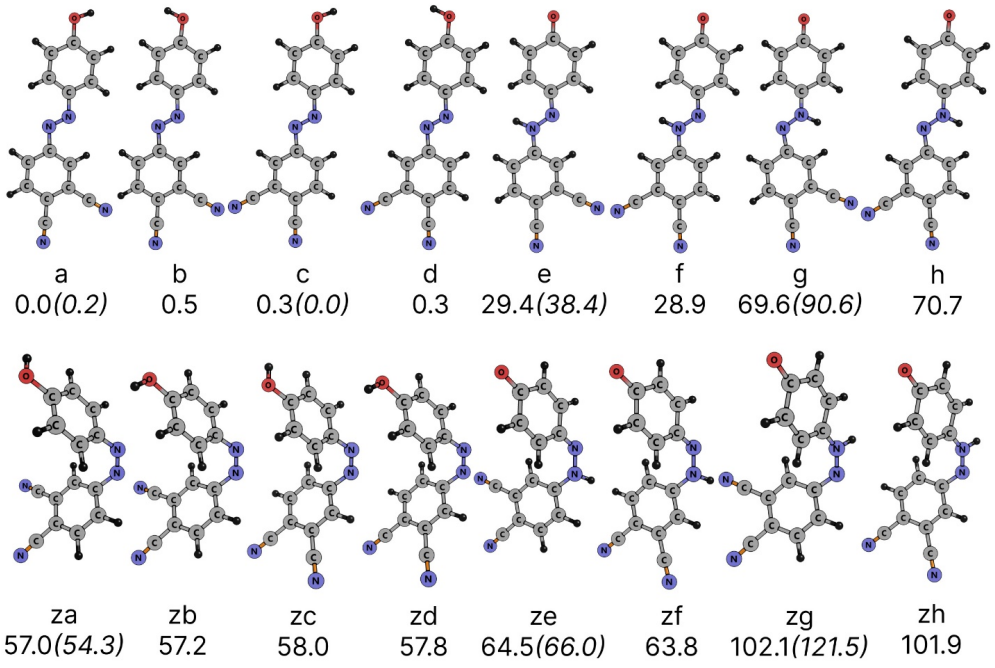

Figure 3. Conformer and isomer models of ***p-HPhAPN***. Appropriate relative energies (kJ·mol^{-1}) obtained using B3LYP-D3/pcseg-2 (DLPNO-CCSD(T0)/CBS // B3LYP-D3/pcseg-2 - italic in brackets) calculations are indicated.

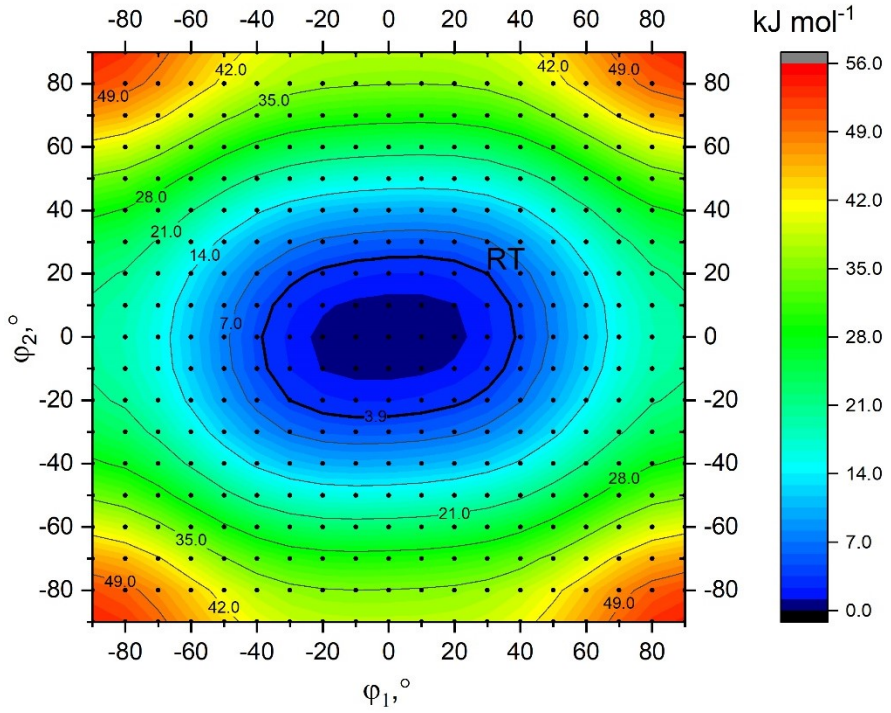

Figure 4. Potential energy surface (PES) obtained at the B3LYP-D3/pcseg-2 level of theory as a function of rotations of –Ph-2CN and –Ph-OH moieties around N1-C2 (φ_1) and N1'-C2' (φ_2) bonds (see Figure 1). Bold line RT corresponds to the temperature of the GED experiment (T_{exp}=464 K). Black circles indicate the calculations performed for the corresponding values of angles.

Potential energy surface

Parent ***AB*** has a soft energy surface along the phenyl torsional coordinate.[15] This is also typical for ***p-HPhAPN*** (Figure 4). However, the rotations of different rings are not the same. The rotation of the phenolic fragment is energetically more hindered. According to DLPNO-CCSD(T0)/CBS // B3LYP-D3/pcseg-2 calculations, the ring rotation barrier substituted by the -OH group is *ca.* 28 kJ·mol^{-1}. For rotation of –Ph-2CN around N1-C2 bond the barrier is *ca.* 17 kJ·mol^{-1}. These differences can be explained by the fact that the conjugation between the phenolic group and the azo bridge is greater than in the case of interaction between the azo bridge and the phthalonitrile fragment. It was confirmed by NBO analysis earlier[17] and by NICS criteria in this study (Table S7). It is known that to form a large aromatic system through several moieties, the aromaticity of separate rings should be decreased or lost.[74] NICS(1) for –Ph-2CN moiety is –8.7 whereas the value for –Ph-OH fragment is –7.9. It should be noted, that B3LYP-D3/pcseg-2 calculations overestimate the values of rotation barriers for –Ph-OH and –Ph-2CN by *ca.* 10 and 3 kJ·mol^{-1} compared to DLPNO-CCSD(T0)/CBS calculations (Figure 4). In addition, for ***p-HPhAPN***, rotation of -OH group along the bond C-O is possible. According to DLPNO-CCSD(T0)/CBS // B3LYP-D3/pcseg-2 calculations, the barrier of –OH group rotation amounts to 17 kJ·mol^{-1}.

*Fragmentation of **p-HPhAPN***

To analyze the experimental mass spectra of ***p-HPhAPN***, theoretical QCxMS calculations were used. The applicability of the theoretical approach to this case was assessed using the parent ***AB***. The EI-MS of ***AB*** known in literature[75-77] was represented by several peaks corresponding to molecular ion with *m/z*=182 (relative intensity *I* is ~30%) and ions formed due to fragmentation. The predominant process under electron impact is the destruction of the N-C bonds, resulting in the formation of cations [Ph-N=N]$^{+\cdot}$ and [Ph]$^{+\cdot}$.[78] As a result, the EI-MS contains 2 peaks (*m/z*=105 and 77), the relative intensities *I* of which are ~20% and 100%, respectively.[75,78] The peak at *m/z*=51 with a relative intensity *I*≈35% corresponds to the ion formed due to fragmentation $[Ph]^{+\cdot} \rightarrow [C_4H_3]^{+} + H_2C_2$.[78] These fragmentation paths were well reproduced by the QCxMS technique (Figure S2), but the relative abundance *I* of molecular ion was overestimated, as is typical for such calculations.[79] Theoretical calculations for ***AB*** also overestimate intensity corresponding to cyclic and linear chains $[C_6H_5N]^{+\cdot}$ (*m/z*=91), which is almost absent in the experimental spectra[75,78] (Figure S2). The model spectrum also lacks a peak with *m/z*=152 corresponding to skeletal rearrangement ion $[H_4C_6{=}C_6H_4]^{+\cdot}$.[78] Its formation occurs[78,80] as a result of the double bond ionization in the aromatic ring to furnish electron-deficient centers, that are available for the attack of the incipient radical. It is also worth noting that QCxMS procedures started separately for ***E-AB*** and ***Z-AB*** structures yielded similar spectra (Figure S3).

p-HPhAPN undergoes dissociative ionization under the influence of electron impact. As with the parent ***AB***, the predominant processes upon electron impact are the destruction of chemical bonds N1-C2. The most intense peak in the mass spectrum corresponds to the [Ph-OH]$^{+\cdot}$ cation (*m/z*=93). Other intense peaks correspond to the molecular cation (*m/z*=248) and ions [NN-Ph-OH]$^{+\cdot}$ (*m/z*=121). This assignment is consistent with the results of

GFN2-xTB simulated EI-MS. It is worth noting that the QCxMS calculations did not allow us to predict an intense peak with *m/z*=65. This peak may correspond to the structure $[C_5H_5]^{+\cdot}$ obtained by skeletal rearrangement processes with loss of carbon monoxide from $[Ph\text{-}OH]^{+\cdot}$ fragment. A similar signal was recorded in the case of monohydroxyazobenzene.[78] The fragment $[2CN\text{-}Ph]^{+\cdot}$ obtained by to N1-C1 bond cleavage corresponds to a weak peak with *m/z*=127 in the EI-MS. As in the case of ***AB***, QCxMS procedures initiated separately for *trans*- and *cis*- structures yielded similar spectra (Figure S4). In the case of considering the keto structure ***e*** of ***p-HPhAPN***, the theoretical EI-MS does not contain a peak with *m/z*=93, which is predicted for structure ***a*** and observed in the experiment (Figures 4, S5).

*The structure of **p-HPhAPN** according to GED experiment*

According to QC calculations the structures ***a-d*** coexist in approximately equal quantities (Figure S6). The cisoid/transoid arrangement of the nitrile groups relative to the azo bridge affects distances >4 Å between non-bonded atoms (*e.g.*, models ***a*** and ***c***, Figures 3, S1). In this regard, such conformers are difficult to distinguish in GED experiment. The hydrogen atom position could not be determined accurately by the GED method.[81] This means that structures differing only by locations of the hydrogen atom of hydroxyl group will be indistinguishable in the gas phase (*e.g.*, models ***a*** and ***b***, Figures 3, S1) basing GED experiment.

Despite the softness of PES shown in Figure 4, rotation barriers of phenyl and hydroxyl groups (see the section *Potential energy surface*) exceed thermal energy RT, *i.e.* conformational transitions ***a*→*c***, ***a*→*b***, *etc.* do not occur under the experimental conditions. Recent GED studies of ***E-AB*** have shown that the uncertainty in determining the angles φ is about 40°. At the same time, the structural analysis using a dynamic model is redundant for parent ***E-AB***. Therefore, in this work we used only semi-rigid models in GED structural analysis.

The LS analysis of GED experimental intensities was started under the assumption that the vapor contains azo tautomers ***a***, ***c*** and hydrozone tautomers ***e***, ***f***. Separate using models ***a*** and ***c*** allows to achieve acceptable agreement between experimental and theoretical data with wR_d = 4.8% and 5.0%, respectively (Figure S7). Carrying out structural analysis under the assumption that the vapor consists of ***a*** and ***c*** conformers allows, albeit slightly (~0.05%), to reduce the disagreement factor at a 50/50 molar percentage ratio. The models of pure hydrazone forms ***e*** and ***f*** allows to achieve the bad agreement with experimental diffraction intensities with wR_d = 7.2% and 7.3% (Figure S8). Considering a mixture of azo and hydrazone forms (two forms ***c*** and ***f*** together or four forms ***a***, ***c***, ***e***, ***f*** together) leads to an increase in the wR_d. Thus, in the gas phase ***p-HPhAPN*** is presented in the azo forms. Apparently, both cisoid and transoid variants of cyano groups' location are equally probable and all four conformers ***a-d*** are presented in the gas phase. The comparison of the experimental functions *sM(s)* and *f(r)* with the theoretical curves for the mixture of ***a*** and ***c*** with mole ratio 1:1 are shown in Figures 5-6. Table 1 shows that the semi-experimental equilibrium geometric parameters of ***a*** and ***c*** agree satisfactorily with the calculated structural parameters.

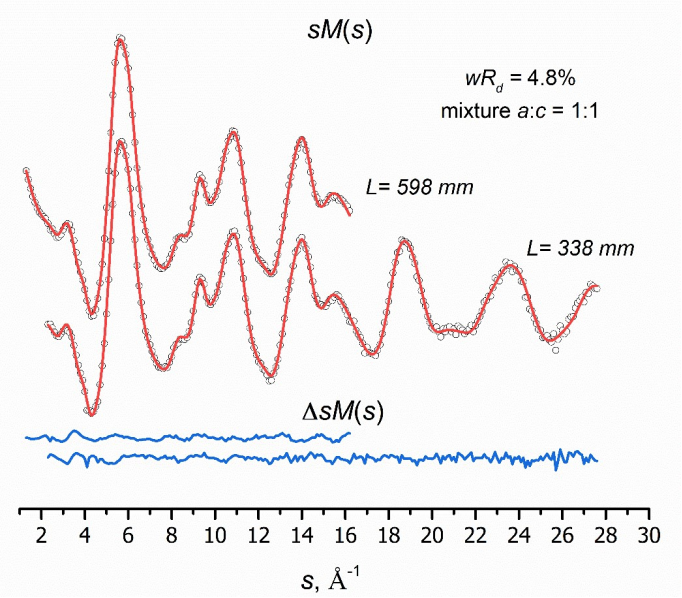

Figure 5. Experimental (cycles) and theoretical (red solid lines) molecular scattering intensities *sM(s)* for mole percent of 50/50 ***a***/***c*** vapor model of ***p-HPhAPN*** and the difference curves Δ*sM(s)* (blue solid lines).

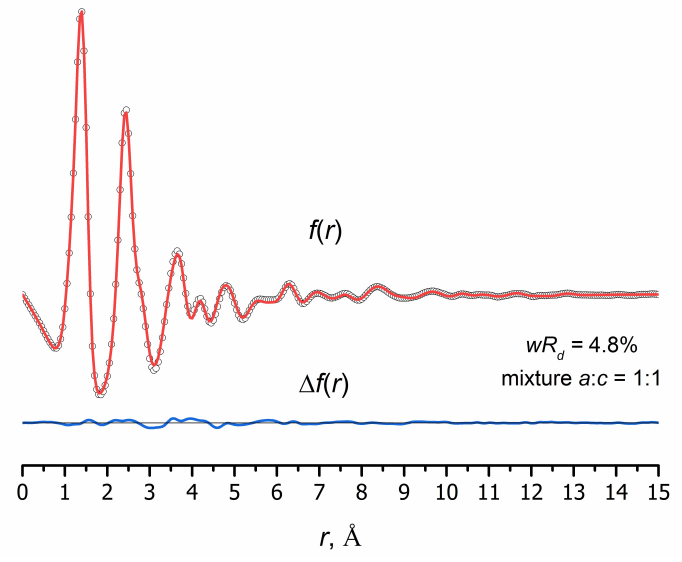

Figure 6. Experimental (cycles) and theoretical (red solid lines) radial distribution curve for mole percent of 50/50 ***a***/***c*** vapor model of ***p-HPhAPN*** and the difference curve Δ*f(r)* (blue solid line).

Table 1. Semi-experimental and theoretical r_e parameters[a] of ***p-HPhAPN*** (azo forms ***a*** and ***c***).

	GED[b] wR_d = 4.8 %		B3LYP-D3/pcseg-2	
	a	***c***	***a***	***c***
N1-N1'	1.250(8)	1.250(8)	1.252	1.252
N1-C2	1.415(11)	1.415(11)	1.414	1.414
N1'-C2'	1.396(11)	1.397(11)	1.400	1.400
C4-C_{CN}	1.434(11)	1.433(11)	1.427	1.426
C5-C_{CN}	1.432(11)	1.432(11)	1.430	1.429
C5'-O	1.331(10)	1.331(10)	1.356	1.356
C-C ave	1.398(11)	1.398(11)	1.396	1.396
C'-C' ave	1.388(11)	1.388(11)	1.393	1.393
C-H ave	1.083(12)	1.083(12)	1.081	1.080
O-H	0.961(12)	0.961(12)	0.962	0.962
N1'-N1-C2	114.9(12)	114.9(12)	114.8	114.8
N1-C2-C3	124.1(13)	115.2(13)	124.4	115.4
N1-C2-C7	117.3(18)	126.2(18)	115.9	124.9
N1-N1'-C2'	116.3(11)	116.1(11)	116.4	116.3
N1'-C2'-C3'	125.4(10)	125.3(10)	125.0	124.9
N1'-C2'-C7'	116.1(17)	116.2(17)	115.7	115.7
C3-C2-C7	118.5(13)	118.6(13)	119.7	119.7
C6-C5-C_{CN}	122.9(12)	123.0(12)	121.1	121.2
C4-C5-C_{CN}	117.6(13)	117.5(13)	119.7	119.5
C3'-C2'-C7'	118.5(13)	118.5(13)	119.4	119.3
C4'-C5'-O	116.7(13)	116.7(13)	116.9	116.9
C6'-C5'-O	122.8(14)	122.8(14)	122.8	122.8

[a]internuclear distances in Å, bond angles in °, a complete list of structural parameters is given in the Table S9;
[b]uncertainties for the bond lengths were estimated as $[(2.5\sigma_{LS})^2 + (0.002r)^2]^{1/2}$; uncertainty for the angle was estimated as $3\sigma_{LS}$.

Structures of phthalocyanines

We also consider the structures of zinc phthalocyanine complexes, which can be obtained from ***p-HPhAPN***. Figure 7 shows several isomers of zinc(II) tetra-4-[(E)-(4'-hydroxyphenyl)diazenyl]phthalocyanine (***Zn-tHPhDaPc***). The structures of ***Zn-tHPhDaPc*** formed only by one of the forms ***a***, ***c***, ***e***, ***f*** are considered. According to B3LYP-D3/pcseg-2 calculations, the ***Zn-tHPhDaPc*** formed from ***c*** is slightly lower in energy than the complex obtained by ***a*** (Table S10). The differences in internuclear distances of these conformers are insignificant (do not exceed 0.006 Å) and relate only to the phenyl fragment of the phthalocyanine core (Table S11). Analyzing the values of internuclear distances and values of NICS criteria (Tables S7, S12), it is noted that the structure of the phenyl rings of the original ***p-HPhAPN*** changes slightly during the formation of the phthalocyanine macrocycle. The hydrazone form of the complex is unfavorable compared to the azo form. The energy difference is 104 kJ·mol^{-1}, which corresponds to 26 kJ·mol^{-1} per 1 azo/hydrazone substituent (energy difference between tautomers ***a*** and ***e*** is 29 kJ·mol^{-1}, see Figure 3). Thus, the tautomeric features of the macrocycle are apparently the same as those of the parent phthalonitrile.

Conclusions

The ***p-HPhAPN*** is thermally stable up to at least 487 K, as evidenced by the data of the EI-MS experiments. Registered EI-MS are typical for azobenzenes and are interpreted quite well using the results of QCxMS calculations at the GFN2-xTB level of theory. However, the work also noted some differences between experimental and theoretical EI-MS.

Sixteen possible structures of ***p-HPhAPN*** were studied by QC calculations. Such a large number of models is due to the possibility of *cis-trans* isomerism, azo-hydrazone tautomerism, rotations of different moieties in the molecule. Based on DFT and DLPNO-CCSD(T0) calculations and GED experiment, the compound has planar structure and is in the azo form. Apparently the forms with different (cisoid/transoid) arrangement of nitrile groups with respect to the azo group coexist in approximately equal proportions, and this circumstance can make difficult growing the monocrystal. Hydrazone isomers have higher energy and their concentration in vapor at moderate temperatures appears to be negligible.

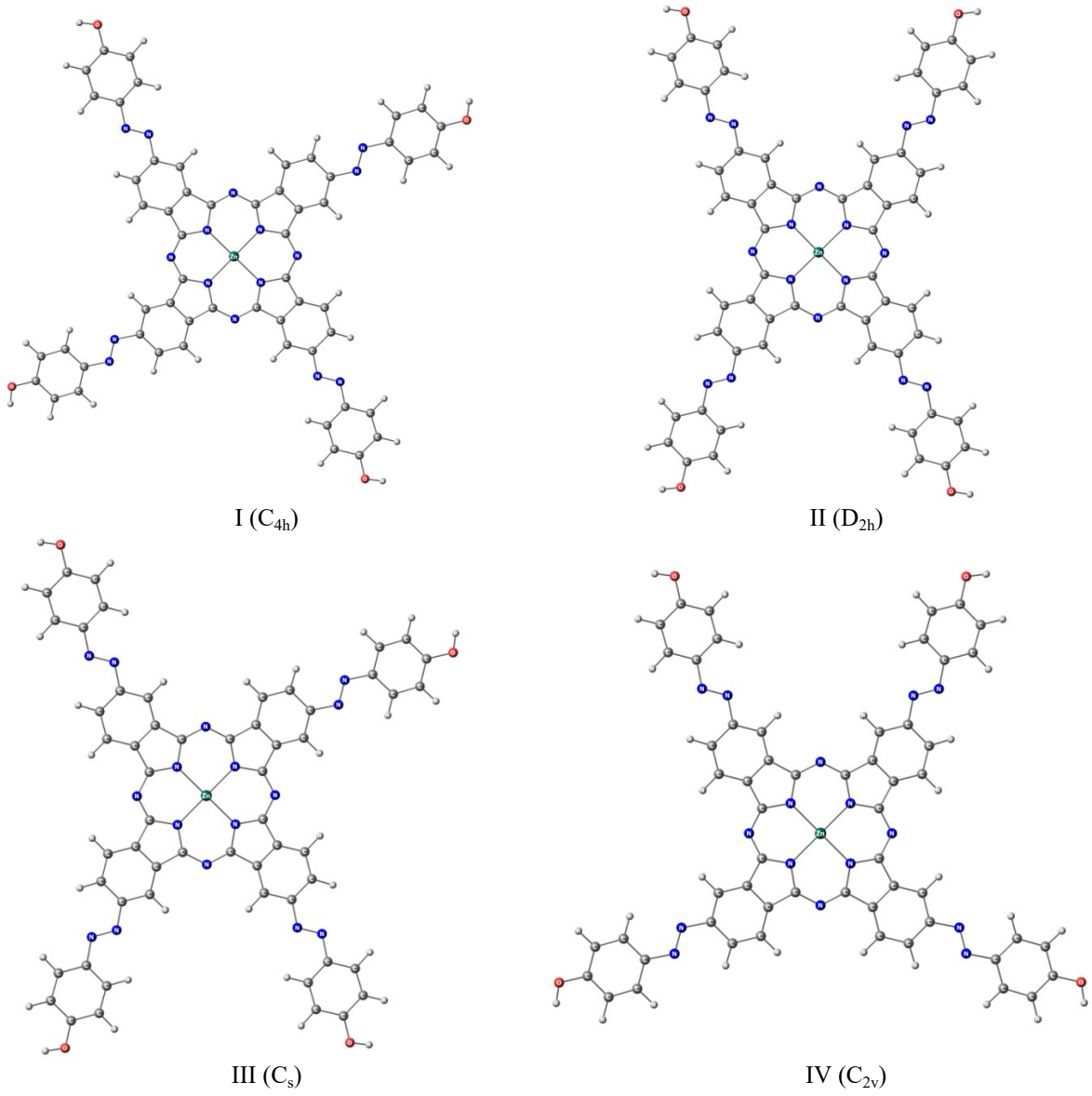

Figure 7. Isomers I-IV of ***Zn-tHPhDaPc*** obtained from only *a* forms of ***p-HPhAPN***.

The equilibrium geometrical r_e parameters of ***p-HPhAPN*** free molecule were refined by GED data. The possibility for correct comparison of experimental and theoretical data appears due to both semi-experimental and theoretical structural parameters have identical physical sense. The close coincidence of semi-experimental geometrical parameters of ***p-HPhAPN*** with the calculated ones (Table 1) allow recommending the theory level B3LYP-D3/pcseg-2 for calculations of structure and vibrational spectra of substituted azo-phthalonitriles. The ***p-HPhAPN*** compound is promising for use as a precursor in the synthesis of various metal phthalocyanines with a large effective area and ideal flatness. In turn, such metal phthalocyanine complexes can be suitable for obtaining discotic liquid crystals with close packing of neighboring molecules.

Funding. The study was supported by the Russian Science Foundation (grant No. 22-73-00314).

Acknowledgements. The GED/MS experiments were carried out using the GED/MS equipment of the resources of the Center for Shared Use of Scientific Equipment of the ISUCT (*https://www.isuct.ru/department/ckp/structure/ged-ms*, accessed Febr. 14, 2024).

Supplementary materials. The following are available online: Table S1. Conditions of GED experiments for ***p-HPhAPN***. Table S2. The most intensive ions in the mass spectrum of ***p-HPhAPN*** were recorded by APDM-1 during the combined GED/MS experiment. Figure S1. Comparison of theoretical radial distribution functions *f*(r) of different structures of ***p-HPhAPN***. Table S3. Z-matrix used for model ***c*** in the GED refinement. Table S4. Z-matrix used for model ***a*** in the GED refinement. Table S5. Z-matrix used for model ***e*** in the GED refinement. Table S6. Z-matrix was used for model ***f*** in the GED refinement. Table S7. Nucleus-independent chemical shifts (NICS) indexes for ***E-AB*** and ***p-HPhAPN***. Table S8. Electron delocalization indexes calculated by QTAIM for several structures of ***p-HPhAPN***. Figure S2. Calculated (GFN2-xTB) EI-MS of ***E-AB*** in comparison with the experimental EI-MS. Figure S3. Comparison of EI-MS obtained using the QCxMS (GFN2-

xTB) procedures started separately for ***E-AB*** and ***Z-AB*** structures. Figure S4. Comparison of EI-MS obtained using the QCxMS (GFN2-xTB) procedures started separately for ***E-AB*** and ***Z-AB*** structures. Figure S5. Comparison of calculated (GFN2-xTB) EI-MS of ***p-HPhAPN*** isomers ***a*** and ***e***. Figure S6. Temperature dependence of conformational/isomeric composition of ***p-HPhAPN***. Figure S7. Experimental and theoretical radial distribution curve models ***c*** and ***a*** of ***p-HPhAPN*** and the difference curve $\Delta f(r)$. Figure S8. Experimental and theoretical radial distribution curve for models ***f*** and ***e*** of ***p-HPhAPN*** and the difference curve $\Delta f(r)$. Table S9. Semi-experimental parameters of ***p-HPhAPN*** (azo forms ***a*** and ***c***). Table S10. Relative energies of different isomers of ***Zn-tHPhDaPc*** obtained using different forms (***a***, ***c***, ***e***, ***f***) of ***p-HPhAPN***. Table S11. Internuclear distances of zinc complex ***Zn-tHPhDaPc,*** obtained using ***a*** and ***c*** forms of ***p-HPhAPN,*** and corresponding internuclear distances of ***p-HPhAPN*** (models ***a*** and ***c***). Table S12. Nucleus-independent chemical shifts indexes for zinc phtalocyanine and ***Zn-tHPhDaPc***. Additionally, semi-experimental GED equilibrium structures and optimized structures from QC calculations at B3LYP-D3/pcseg-2 levels are given in Supplementary Materials (available on https://doi.org/10.6060/mhc245112p).

References

1. Ali Y., Hamid A.S., Rashid U. *Mini-Reviews Med. Chem.* **2018**, *18*, 1548–1558.
2. Bafana A., Devi S.S., Chakrabarti T. *Environ. Rev.* **2011**, *19*, 350–371.
3. Fedele C., Ruoko T.-P., Kuntze K., Virkki M., Priimagi A. *Photochem. Photobiol. Sci.* **2022**, *21*, 1719–1734.
4. Giles L.W., Faul C.F.J., Tabor R.F. *Mater. Adv.* **2021**, *2*, 4152–4164.
5. Purkait M.K., Sinha M.K., Mondal P., Singh R. Photoresponsive Membranes. In: *Stimuli Responsive Polymeric Membranes, Ch. 4* (Purkait M.K., Sinha M.K., Mondal P., Singh R., Eds.), Academic Press, Elsevier, **2018**. pp. 115–144.
6. Natansohn A., Rochon P. *Chem. Rev.* **2002**, *102*, 4139–4176.
7. Manickasundaram S., Kannan P., Hassan Q.M.A., Palanisamy P.K. *J. Mater. Sci. Mater. Electron.* **2008**, *19*, 1045–1053.
8. Beharry A.A., Woolley G.A. *Chem. Soc. Rev.* **2011**, *40*, 4422–4437.
9. Mohr G.J., Müller H., Bussemer B., Stark A., Carofiglio T., Trupp S., Heuermann R., Henkel T., Escudero D., González L. *Anal. Bioanal. Chem.* **2008**, *392*, 1411–1418.
10. Shikhaliyev N.Q., Kuznetsov M.L., Maharramov A.M., Gurbanov A.V., Ahmadova N.E., Nenajdenko V.G., Mahmudov K.T., Pombeiro A.J.L. *CrystEngComm* **2019**, *21*, 5032–5038.
11. Naime J., Al Mamun M.S., Aly Saad Aly M., Maniruzzaman M., Badal M.M.R., Karim K.M.R. *RSC Adv.* **2022**, *12*, 28034–28042.
12. Lee H.Y., Song X., Park H., Baik M.-H., Lee D. *J. Am. Chem. Soc.* **2010**, *132*, 12133–12144.
13. Wang X. *Trans-Cis* Isomerization. In: *Azo Polymers. Soft and Biological Matter.* Springer Berlin Heidelberg, Berlin, Heidelberg, **2017**. pp. 19–56. Springer, Berlin, Heidelberg.
14. Tiago M.L., Ismail-Beigi S., Louie S.G. *J. Chem. Phys.* **2005**, *122*, 94311.
15. Duarte L., Fausto R., Reva I. *Phys. Chem. Chem. Phys.* **2014**, *16*, 16919–16930.
16. Fliegl H., Köhn A., Hättig C., Ahlrichs R. *J. Am. Chem. Soc.* **2003**, *125*, 9821–9827.
17. Pogonin A.E., Kurochkin I.Y., Malyasova A.S., Ksenofontova K.V., Koifman O.I. *Macroheterocycles* **2023**, *16*, 156–167.
18. Mahimwalla Z., Yager K.G., Mamiya J., Shishido A., Priimagi A., Barrett C.J. *Polym. Bull.* **2012**, *69*, 967–1006.
19. Shishido A. *Polym. J.* **2010**, *42*, 525–533.
20. Chang V.Y., Fedele C., Priimagi A., Shishido A., Barrett C.J. *Adv. Opt. Mater.* **2019**, *7*, 1900091.
21. Kishimoto S., Kitahara S., Manabe O., Hiyama H. *J. Org. Chem.* **1978**, *43*, 3882–3886.
22. Ball P., Nicholls C.H. *Dyes Pigm.* **1982**, *3*, 5–26.
23. Özen A.S., Doruker P., Aviyente V. *J. Phys. Chem. A* **2007**, *111*, 13506–13514.
24. Steinwand S., Halbritter T., Rastädter D., Ortiz-Sánchez J.M., Burghardt I., Heckel A., Wachtveitl J. *Chem. – A Eur. J.* **2015**, *21*, 15720–15731.
25. Ngororabanga J.M.V., Dembaremba T.O., Mama N., Tshentu Z.R. *Spectrochim. Acta, Part A Mol. Biomol. Spectrosc.* **2023**, *289*, 122202.
26. Adegoke O.A., Adesuji T.E., Thomas O.E. *Spectrochim. Acta, Part A Mol. Biomol. Spectrosc.* **2014**, *128*, 147–152.
27. Baldini L., Balestri D., Marchiò L., Casnati A. *Molecules* **2023**, *28*, 4704.
28. Demaison J., Vogt N. Molecular Structures from Gas-Phase Electron Diffraction. In: *Accurate Structure Determination of Free Molecules*, Springer International Publishing, Cham, **2020**. pp. 167–204.
29. Girichev G.V., Giricheva N.I., Kudin L.S., Solomonik V.G., Belova N.V., Butman M.F., Vyalkin D.A., Dunaev A.M., Eroshin A.V., Zhabanov Y.A., Krasnov A.V., Kuzmina L.E., Kuzmin I.A., Kurochkin I.Y., Motalov V.B., Navarkin I.S., Pimenov O.A., Pogonin A.E., Sliznev V.V., Smirnov A.N., Tverdova N.V., Shlykov S.A. *ChemChemTech [Izv. Vyssh. Uchebn. Zaved. Khim. Khim. Tekhnol.]* **2023**, *66*(7), 11–30.
30. Traetteberg M., Hillmo I., Hagen K. *J. Mol. Struct.* **1977**, *39*, 231–239.
31. Tsuji T., Takashima H., Takeuchi H., Egawa T., Konaka S. *J. Phys. Chem. A* **2001**, *105*, 9347–9353.
32. Tikhomirova T.V., Znoiko S.A., Shaposhnikov G.P. *Russ. J. Gen. Chem.* **2018**, *88*, 1164–1171.
33. Han M., Zhang X., Zhang X., Liao C., Zhu B., Li Q. *Polyhedron* **2015**, *85*, 864–873.
34. de la Torre G., Bottari G., Hahn U., Torres T. Functional Phthalocyanines: Synthesis, Nanostructuration, and Electro-Optical Applications. In: *Functional Phthalocyanine Molecular Materials* (Jiang J., Ed.), Springer Berlin Heidelberg, Berlin, Heidelberg, **2010**. pp. 1–44.
35. Claessens C.G., Hahn U., Torres T. *Chem. Rec.* **2008**, *8*, 75–97.
36. Wöhrle D., Schnurpfeil G., Makarov S.G., Kazarin A., Suvorova O.N. *Macroheterocycles* **2012**, *5*, 191–202.
37. Zhang Y., Lovell J.F. *WIREs Nanomedicine and Nanobiotechnology* **2017**, *9*, e1420.
38. Tverdova N.V., Giricheva N.I., Maizlish V.E., Galanin N.E., Girichev G.V. *Int. J. Mol. Sci.* **2022**, *23*, 13922.
39. Tverdova N.V., Giricheva N.I., Maizlish V.E., Galanin N.E., Girichev G.V. *Macroheterocycles* **2022**, *15*, 40–43.
40. Tyunina V.V., Krasnov A.V., Badelin V.G., Girichev G.V. *J. Chem. Thermodyn.* **2016**, *98*, 62–70.
41. Girichev G.V., Utkin A.N., Revichev Y.F. *Prib. Tekh. Eksp.* **1984**, *27*, 187–190.
42. Girichev G.V., Shlykov S.A., Revichev Y.F. *Prib. Tekh. Eksp.* **1986**, *29*, 167–169.
43. Girichev E.G., Zakharov A.V., Girichev G.V., Bazanov M.I. *Izv. Vysh. Uchebn. Zaved., Tekst. Prom.* **2000**, *2*, 142–146.
44. Vishnevskiy Y.V., UNEX [version 1.7], *https://unex.vishnevskiy.group* (accessed Jan. 10, 2024)
45. Vishnevskiy Y.V., Zhabanov Y.A. *J. Phys. Conf. Ser.* **2015**, *633*, 012076.
46. Mitzel N.W., Rankin D.W.H. *Dalton Trans.* **2003**, 3650–3662.

47. Vishnevskiy Y.V., Abaev M.A., Rykov A.N., Gurskii M.E., Belyakov P.A., Erdyakov S.Y., Bubnov Y.N., Mitzel N.W. *Chem. - A Eur. J.* **2012**, *18*, 10585–10594.
48. Kochikov I.V., Tarasov Y.I., Kuramshina G.M., Spiridonov V.P., Yagola A.G., Strand T.G. *J. Mol. Struct.* **1998**, *445*, 243–258.
49. Tikhonov D.S., Vishnevskiy Y.V., Rykov A.N., Grikina O.E., Khaikin L.S. *J. Mol. Struct.* **2017**, *1132*, 20–27.
50. Frisch M.J., Trucks G.W., Schlegel H.B., Scuseria G.E., Robb M.A., Cheeseman J.R., Scalmani G., Barone V., Mennucci B., Petersson G.A., Nakatsuji H., Caricato M., Li X., Hratchian H.P., Izmaylov A.F., Bloino J., Zheng G., Sonnenberg J.L., Hada M., Ehara M., Toyota K., Fukuda R., Hasegawa J., Ishida M., Nakajima T., Honda Y., Kitao O., Nakai H., Vreven T., Montgomery J.A.,Jr., Peralta J.E., Ogliaro F., Bearpark M., Heyd J.J., Brothers E., Kudin K.N., Staroverov V.N., Kobayashi R., Normand J., Raghavachari K., Rendell A., Burant J.C., Iyengar S.S., Tomasi J., Cossi M., Rega N., Millam J.M., Klene M., Knox J.E., Cross J.B., Bakken V., Adamo C., Jaramillo J., Gomperts R., Stratmann R.E., Yazyev O., Austin A.J., Cammi R., Pomelli C., Ochterski J.W., Martin R.L., Morokuma K., Zakrzewski V.G., Voth G.A., Salvador P., Dannenberg J.J., Dapprich S., Daniels A.D., Farkas O., Foresman J.B., Ortiz J.V., Cioslowski J., Fox D.J. *Gaussian 09, Revision D.01,* Gaussian, Inc., Wallingford CT, **2009**.
51. Becke A.D. *J. Chem. Phys.* **1993**, *98*, 5648–5652.
52. Lee C., Yang W., Parr R.G. *Phys. Rev. B* **1988**, *37*, 785.
53. Grimme S., Antony J., Ehrlich S., Krieg H. *J. Chem. Phys.* **2010**, *132*, 154104.
54. Jensen F. *J. Chem. Theory Comput.* **2014**, *10*, 1074–1085.
55. Pritchard B.P., Altarawy D., Didier B., Gibson T.D., Windus T.L. *J. Chem. Inf. Model.* **2019**, *59*, 4814–4820.
56. Notes about the Jensen basis sets, *https://www.basissetexchange.org/family_notes/jensen/* (accessed April 8, 2024).
57. Pitman S.J., Evans A.K., R Ireland.T., Lempriere F., McKemmish L.K. *J. Phys. Chem. A* **2023**, *127*, 10295–10306.
58. Keith T.A. *AIMAll (Version 19.10.12),* **2017**, *http://aim.tkgristmill.com/* (accessed May 14, 2021).
59. Liakos D.G., Guo Y., Neese F. *J. Phys. Chem. A* **2020**, *124*, 90–100.
60. Saitow M., Becker U., Riplinger C., Valeev E.F., Neese F. *J. Chem. Phys.* **2017**, *146*, 164105.
61. Riplinger C., Neese F. *J. Chem. Phys.* **2013**, *138*, 34106.
62. Riplinger C., Sandhoefer B., Hansen A., Neese F. *J. Chem. Phys.* **2013**, *139*, 134101.
63. Neese F., Wennmohs F., Becker U., Riplinger C. *J. Chem. Phys.* **2020**, *152*, 224108.
64. Minenkov Y., Bistoni G., Riplinger C., Auer A.A., Neese F., Cavallo L. *Phys. Chem. Chem. Phys.* **2017**, *19*, 9374–9391.
65. Bruno G., de Souza B., Neese F., Bistoni G. *Phys. Chem. Chem. Phys.* **2022**, *24*, 14228–14241.
66. Dunning T.H. *J. Chem. Phys.* **1989**, *90*, 1007–1023.
67. Martin J.M.L. *Chem. Phys. Lett.* **1996**, *259*, 669–678.
68. Minenkov Y., Cavallo L., Peterson K.A. *J. Comput. Chem.* **2023**, *44*, 687–696.
69. Weigend F., Köhn A., Hättig C. *J. Chem. Phys.* **2002**, *116*, 3175–3183.
70. Grimme S. *Angew. Chem. Int. Edit.* **2013**, *52*, 6306–6312.
71. Koopman J., Grimme S. *ACS Omega* **2019**, *4*, 15120–15133.
72. Bannwarth C., Ehlert S., Grimme S. *J. Chem. Theory Comput.* **2019**, *15*, 1652–1671.
73. Giricheva N.I., Lebedev I.S., Fedorov M.S., Bubnova K.E., Girichev G.V. *J. Struct. Chem.* **2021**, *62*, 1976–1987.
74. Islyaikin M.K., V Ferro.R., García de la Vega J.M. *J. Chem. Soc., Perkin Trans. 2* **2002**, *17*, 2104–2109.
75. In: *NIST Chemistry WebBook*, NIST Standard Reference Database Number 69, National Institute of Standards and Technology.
76. Moran M.J., Martina K., Baricco F., Tagliapietra S., Manzoli M., Cravotto G. *Adv. Synth. \Catal.* **2020**, *362*, 2689–2700.
77. Zhang C., N. Jiao, *Angew. Chem. Int. Edit.* **2010**, *49*, 6174–6177.
78. Bowie J.H., Lewis G.E., Cooks R.G. *J. Chem. Soc. B* **1967**, 621–628.
79. Schreckenbach S.A., Anderson J.S.M., Koopman J., Grimme S., Simpson M.J., Jobst K.J. *J. Am. Soc. Mass Spectrom.* **2021**, *32*, 1508–1518.
80. Bowie J.H., Lawesson S.O., Madsen J.Ø., Nolde C., Schroll G., Williams D.H. *J. Chem. Soc. B* **1966**, 946–951.
81. Vogt N., Savelev D., Giricheva N.I., Girichev G.V. *Phys. Chem. Chem. Phys.* **2020**, *22*, 27539–27546.

Received 03.04.2024
Accepted 28.04.2024